Journal of Power Sources 196 (2011) 4816–4820

Contents lists available at ScienceDirect

Journal of Power Sources

journal homepage: www.elsevier.com/locate/jpowsour

Short communication

Graphite materials prepared by HTT of unburned carbon from coal combustion fly ashes: Performance as anodes in lithium-ion batteries

Ignacio Cameán, Ana B. Garcia*

Instituto Nacional del Carbón, Química Ambiental, CSIC, Francisco Pintado Fe 26, 33011 Oviedo, Spain

ARTICLE INFO

Article history:
Received 2 August 2010
Received in revised form 7 January 2011
Accepted 16 January 2011
Available online 26 January 2011

Keywords:
Graphite material
Anode
Lithium-ion battery
Unburned carbon
Coal fly ashes

ABSTRACT

The behaviour as the potential negative electrode in lithium-ion batteries of graphite-like materials that were prepared by high temperature treatment of unburned carbon concentrates from coal combustion fly ashes was investigated by galvanostatic cycling. Emphasis was placed on the relation between the structural/morphological and electrochemical characteristics of the materials. In addition, since good electrode capacity retention on cycling is an important requirement for the manufacturing of the lithium-ion batteries, the reversible capacity provided by the materials prepared on prolonged cycling (50 cycles) was studied and the results were compared with those of petroleum-based graphite which is commercialized as anodic material for lithium-ion batteries. The graphite-like materials prepared lead to battery reversible capacities up to ~310 mA hg^{-1} after 50 cycles, these values were similar to those of the reference graphite. Moreover, they showed a remarkable stable capacity along cycling and low irreversible capacity. Apparently, both the high degree of crystallinity and the irregular particle shape with no flakes appear to contribute to the good anodic performance in lithium-ion batteries of these materials, thus making feasible their utilization to this end.

1. Introduction

Graphite with relatively high specific capacity, high cycling efficiency and low irreversible charge are nowadays the choice of a majority of the commercially available lithium-ion batteries which are currently the energy source for most of the portable electronic devices [1]. The global demand for mobile energy storage systems such as lithium-ion batteries are expected to grow due to the manufacturing of the electric vehicles, thus affecting the graphite market both in terms of production and price [2].

The production of graphite involves the selection of carbon materials that graphitize readily. Currently, petroleum coke is used as the main precursor material in the manufacturing of synthetic graphite [3]. Different factors, however, have drawn the researcher interests towards the study of other alternative precursors. Among the different classes of coal, anthracites can graphitize when heated at temperatures above 2000 °C [4]. Thus, materials with structural characteristics similar to those of oil-derived graphite were prepared from anthracites by high temperature treatment [4–8]. The electrochemical performance as the potential negative electrode in lithium-ion batteries of graphite materials obtained from Spanish anthracites was, then, investigated by galvanostatic cycling [9]. Excellent battery cyclability as well as low irreversible charge was attained by using these materials. In the other hand, in previous works [10,11], unburned carbon concentrates from anthracite combustion fly ashes showing carbon contents of >90% and lamellar microtexture were heated to explore their ability to graphitize. By using HRTEM, several *stricto sensu* graphite structures with a very high degree of layers parallelism (d_{002} value of 0.3356 nm) and directly measured L_c and L_a values up to 60 nm and 350 nm, respectively, were found in the materials prepared at 2600–2700 °C [11]. Since the reversible electrochemical intercalation of lithium in graphite-like materials is known to depend on their degree of structural order [9,12–15], these results encouraged us to study the performance of coal fly ashes unburned carbon-based graphite materials as electrodes in lithium-ion batteries.

Although it is beyond the scope of this paper, it has been considered worthy to mention that fly ashes are the main solid wastes generated in coal combustion plants with a total production only in the USA in 2007 amounting to ~70×10^6 t [16], their disposal causing several economic and environmental problems worldwide. Since their reuse in the production of concrete and cement (the main route of coal fly ash utilization) is limited by the proportion of unburned carbon present, the separation and further utilization of this carbon material as a precursor for value-added products such as graphite would contribute to offset the above mentioned problems.

In the work described in this paper, the behaviour as the potential negative electrodes in lithium-ion batteries of graphite

* Corresponding author. Tel.: +34 985118954; fax: +34 985297662.
E-mail address: anabgs@incar.csic.es (A.B. Garcia).

0378-7753/$ – see front matter © 2011 Elsevier B.V. All rights reserved.
doi:10.1016/j.jpowsour.2011.01.041

materials of different degree of structural order that were prepared by high temperature treatment of unburned carbon concentrates from coal combustion fly ashes was investigated by galvanostatic cycling. Emphasis was placed on the relation between the structural and electrochemical characteristics of the materials. The interlayer spacing, d_{002}, and crystallite sizes along the *c* axis, L_c, and the *a* axis, L_a, calculated from X-ray diffractometry (XRD) as well as the relative intensity of the Raman D-band, I_D/I_t, are used in this study to assess the degree of structural order of the graphite materials. Both XRD and Raman spectroscopy techniques have been extensively used in the structural characterization of carbon materials [17–19]. In addition, since good electrode capacity retention on cycling is an important requirement for the manufacturing of the lithium-ion batteries, the reversible capacity provided by the materials prepared on prolonged cycling (50 cycles) was studied and the results were compared with those of petroleum-based graphite which is currently commercialized as anodic material for lithium-ion batteries.

2. Materials and methods

2.1. Unburned carbon concentrates: source, preparation and designation

Three unburned carbon concentrates denoted A/CVP, B/CIQ1 and B/CIQ5 were prepared from A or B pulverized coal combustion fly ashes (mainly fed with anthracites) as follows: A/CVP by screening out the ≤80 μm fraction, and B/CIQ1 and B/CIQ5 following an oil agglomeration methodology described previously [20] by using a waste vegetable oil at concentrations of 1 and 5 wt.%, respectively. Unburned carbon contents of 54.64, 78.35 and 68.02 wt.% were determined for A/CVP, B/CIQ1 and B/CIQ5 concentrates, the elemental carbon percentages being ≥95, ≥98 and ≥99 wt.%, respectively [10].

2.2. High temperature treatments of the unburned carbon concentrates

The high temperature treatments of the A/CVP, B/CIQ1 and B/CIQ5 were carried out at 1800, 2000, 2200, 2300, 2400, 2500, 2600 and 2700 °C in a XERION graphite electrical furnace for 1 h under argon flow. The heating rates were 25 °C min^{-1} from room temperature to 1000 °C, 20 °C min^{-1} in the range 1000–2000 °C and 10 °C min^{-1} from 2000 °C to the prescribed temperature. The graphite materials thus prepared were identified by the precursor (unburned carbon concentrate) designation, and the treatment temperature, such as A/CVP/2400 or B/CIQ1//2600.

2.3. Structural, morphological and textural characterization: XRD, Raman spectroscopy, SEM and nitrogen adsorption/desorption isotherms

The diffractograms were recorded in a Bruker D8 powder diffractometer equipped with a göbel mirror in the incident beam and a parallel-slits analyzer in the diffracted beam. Diffraction data were collected by step scanning with a step size of 0.02° 2θ and scan step 3 s. For each sample, three diffractograms were obtained, using a different representative batch of sample for each run. The mean interlayer spacing, d_{002}, was evaluated from the position of the (0 0 2) peak applying Bragg's equation. The mean crystallite sizes, L_c and L_a, were calculated from the (0 0 2) and (1 1 0) peaks, respectively, using the Scherrer formula, with values of $K = 0.9$ for L_c and 1.84 for L_a [21]. The broadening of diffraction peaks due to instrumental factors was corrected with the use of a silicon standard. Typical standard errors of the XRD parameters are <1% and <4% of the reported values for L_c and L_a, respectively; the d_{002} values are much more precise, with standard errors of <0.01%. Raman spectra were obtained in a Raman microspectrometer HR 800 Jobin Yvon Horiba as described previously [9]. The intensity *I* of the Raman bands was measured using a mixed Gaussian–Lorentzian curve-fitting procedure. The relative intensity of the Raman D-band I_D/I_t was calculated with standard errors lower than 8%. The commercial SG synthetic graphite was also analyzed for comparative purposes.

The materials surface morphology were analyzed with scanning electron microscopy (SEM) using a Zeiss DMS-942 microscope.

Nitrogen adsorption/desorption isotherms were measured at 77 K in a Micromeritics ASAP 2420, after outgassing the samples at 250 °C. The specific surface area and the pore volumes were calculated by applying the BET method to the respective nitrogen adsorption isotherm.

2.4. Cell preparation and electrochemical measurements

For the electrochemical measurements, two-electrodes Swagelok-type cells were used. Metallic lithium discs of 12 mm diameter were the counter-electrodes. The working electrodes were prepared by mixing the active material (92 wt.%) and PVDF binder (8 wt.%) in 1-methyl-2-pirrolidone solution. All of the materials prepared were ground to 20 μm top size prior the electrode preparation. The slurry was deposited on a copper foil of 12 mm diameter by airbrushing to obtain a thin and uniform surface coating, and then was vacuum dried at 120 °C for 20–24 h. Finally, it was hydraulically pressed at a pressure of 0.9 t cm^{-2}. Afterwards, the electrode load (active material + binder) and active material content were calculated by weight difference. The electrode load densities were in the range 2.88–4.80 mg cm^{-2}. Glass micro-fiber disks impregnated with 1 M $LiPF_6$ (EC:DEC, 1:1, w/w) electrolyte solution were the electrode separators. All cells were assembled in a MBraun dry box under argon atmosphere and water content below 1 ppm. The galvanostatic cycling was carried out in the 2.1–0.003 V potential range at a constant current of C/10 (corresponding to a capacity of 372 mA hg^{-1} in 10 h) during 50 cycles versus Li/Li$^+$, using a biologic multichannel VMP2/Z potentiostat/galvanostat.

3. Results and discussion

The cycling behaviour of A/CVP/1800-2700, B/CIQ1/2000-2600 and B/CIQ5/1800-2600 electrode materials is presented in Fig. 1a–c. For comparison, that corresponding to the petroleum-based SG synthetic graphite of reference is included in Fig. 1a. Firstly, it is should be remarked that some of the graphite-like materials prepared in this work from the unburned carbon concentrates, specifically A/CVP/2700 and B/CIQ5/2600, have provided reversible capacities similar to SG graphite of reference (approximately 310 mA hg^{-1} after 50 cycles, Fig. 1). Moreover, all of them show a remarkable stable capacity along cycling with capacity keeping values in the range 90–99% after 50 cycles.

Lithium intercalation into the A/CVP/2700 and B/CIQ5/2600 electrode materials takes place in the voltage range below 0.2 V (Fig. 2a). The Li$^+$ insertion profiles of these materials were much the same to that of the reference graphite, SG. As can be appreciated, all of them show three intercalation plateaus, thus being the typical observed with graphite. A comparison of the differential capacity (absolute value, derived from the first cycle discharge data) versus potential plots in Fig. 2b makes this similarity more evident and in addition to the expected peaks at the voltage plateaus of approximately 0.19 V, 0.10 V and 0.06 V, allows to observe another peak of very low intensity at approximately 0.13 V what has been assigned to the coexistence of lithium intercalation stages 3 and 2L. This transition stage was found to appear only in graphitic mate-

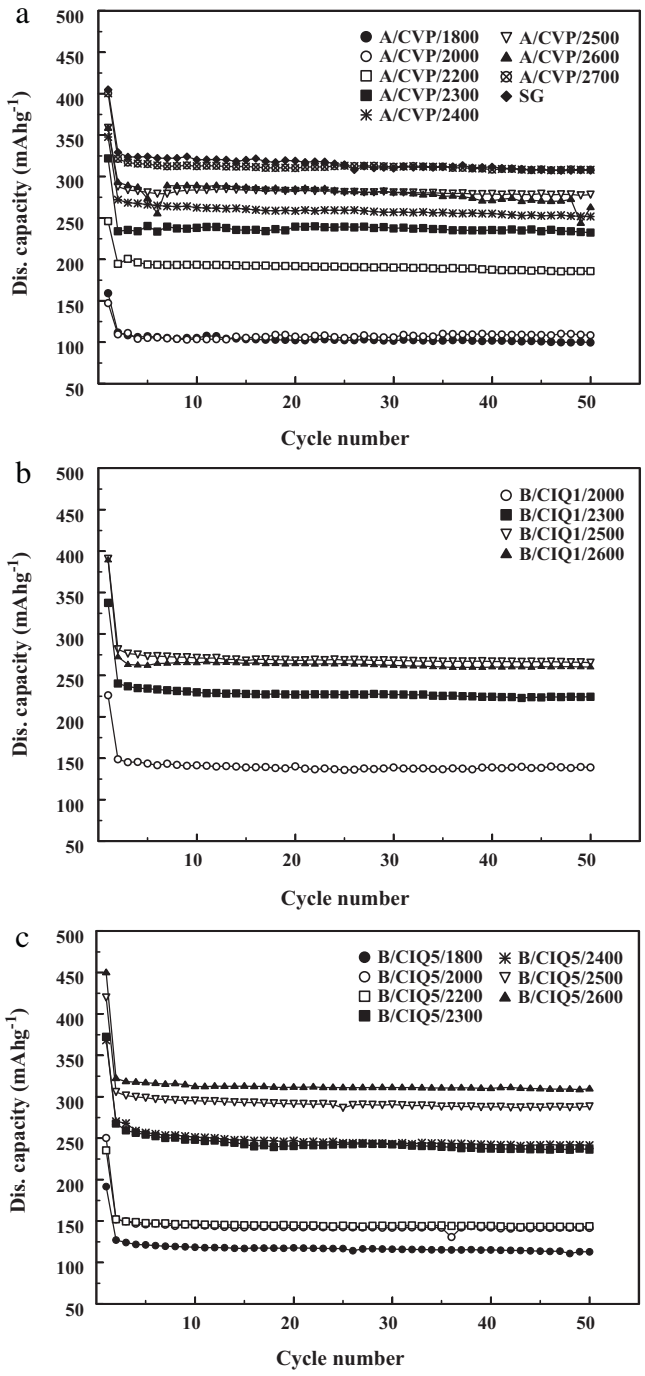

Fig. 1. Extended galvanostatic cycling of A/CVP/1800-2700 and SG (a), of B/CIQ1/2000-2600 (b), and BCIQ5/1800-2600 materials (c).

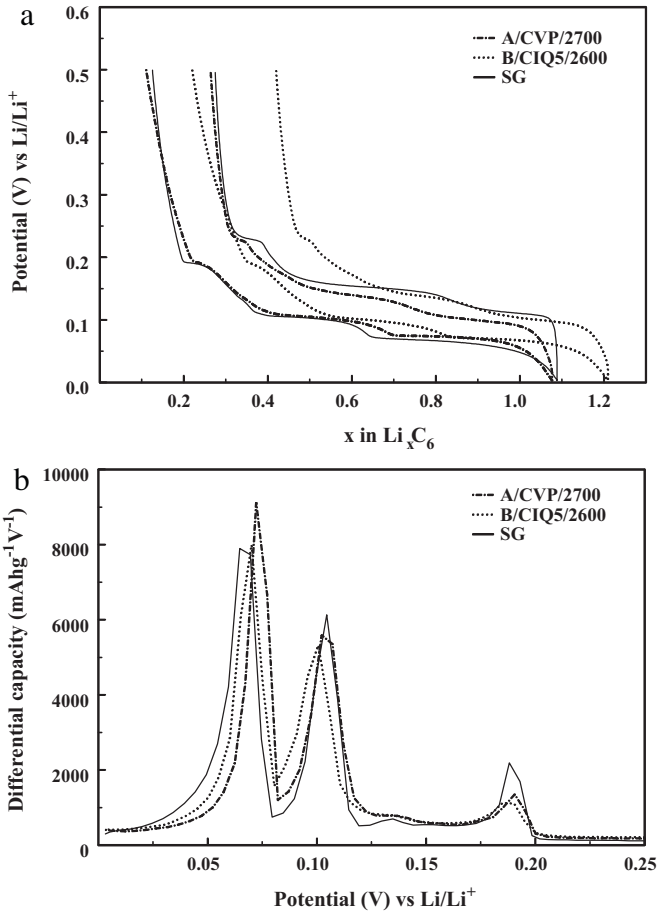

Fig. 2. First Li^+ intercalation/de-intercalation (a) and differential capacity from the first cycle discharge versus potential of A/CVP/2700, B/ClQ5/2600 and SG materials (b).

rials with high degree of crystallinity and structural homogeneity in which disordered carbon phases were not present [22]. In this sense, mainly lamellar graphitic structures were imaged by HRTEM in A/CVP/2700 and B/CIQ5/2600 materials [11].

By comparing the galvanostatic cycling results (Fig. 1) and the XRD and Raman parameters of the materials prepared in Table 1, it is evident that those with higher degree of structural order deliver larger lithium storage capacity. Thus, reversible capacity values of 308 and 185 mA hg^{-1} were calculated after 50 cycles for A/CVP/2700 and A/CVP/2200 electrode materials with crystallite sizes in the c direction L_c of approximately 28 nm and 13 nm, respectively; the corresponding interplanar spacing being

Table 1
Interplanar distance d_{002}, crystallite sizes L_c and L_a, and Raman ratio I_D/I_t of the materials prepared from A/CVP, B/CIQ1 and B/CIQ5 unburned carbon concentrates by HTT and of the SG synthetic graphite of reference.

Material	d_{002} (nm)	L_c (nm)	L_a (nm)	I_D/I_t (%)
A/CVP/1800	0.3419	7.5	–	45.1
A/CVP/2000	0.3412	8.5	–	34.3
A/CVP/2200	0.3390	12.6	–	22.9
A/CVP/2300	0.3378	18.7	–	16.9
A/CVP/2400	0.3382	18.9	–	16.4
A/CVP/2500	0.3372	26.7	52.5	16.0
A/CVP/2600	0.3368	31.0	53.2	12.5
A/CVP/2700	0.3370	27.5	51.2	12.1
B/CIQ1/2000	0.3420	8.8	21.7	42.6
B/CIQ1/2300	0.3389	16.7	44.5	19.4
B/CIQ1/2500	0.3381	20.1	46.9	16.7
B/CIQ1/2600	0.3377	22.6	46.6	15.4
B/CIQ5/1800	0.3420	7.8	–	53.0
B/CIQ5/2000	0.3410	9.3	–	33.9
B/CIQ5/2200	0.3397	11.5	45.9	19.7
B/CIQ5/2300	0.3384	16.7	51.9	17.3
B/CIQ5/2400	0.3382	18.3	50.3	15.9
B/CIQ5/2500	0.3375	23.0	51.2	14.7
B/CIQ5/2600	0.3373	24.8	51.2	14.8
SG	0.3361	50.4	61.1	

Table 2
Textural properties and first cycle irreversible capacity of A/CVP/1800-2700, B/ClQ1/2000-2600 and B/ClQ5/1800-2600 materials and of the synthetic graphite SG.

Material	BET surface area ($m^2\ g^{-1}$)	Total pore volume ($mm^3\ g^{-1}$)	Irreversible capacity ($mA\ hg^{-1}$)	Irreversible capacity (%)
A/CVP/1800	5.9	2.2	58	37
A/CVP/2000	6.2	1.8	46	31
A/CVP/2200	6.2	2.4	62	25
A/CVP/2300	5.5	2.1	48	24
A/CVP/2400	6.3	2.9	85	24
A/CVP/2500	7.1	2.7	85	21
A/CVP/2600	7.1	2.8	75	21
A/CVP/2700	7.5	2.9	86	22
B/ClQ1/2000	5.7	2.1	88	39
B/ClQ1/2300	7.4	2.8	115	34
B/ClQ1/2500	7.1	2.8	127	33
B/ClQ1/2600	8.0	3.1	146	38
B/ClQ5/1800	5.9	2.2	74	39
B/ClQ5/2000	6.2	2.4	110	44
B/ClQ5/2200	7.2	2.8	93	40
B/ClQ5/2300	7.4	2.9	139	37
B/ClQ5/2400	7.7	3.0	125	34
B/ClQ5/2500	8.7	3.4	128	31
B/ClQ5/2600	8.3	3.2	142	32
SG	3.1	1.2	94	23

0.3370 nm and 0.3390 nm. The variation with the relative intensity of the D Raman band I_D/I_t follows a similar tendency. The decrease of this Raman band is related to the improvement of both the degree of structural order and the crystalline orientation of the materials [17–19,23]. To explore a possible correlation between the reversible capacity and the crystallinity of the electrode-forming materials, linear regression analysis were performed with the data appearing in Table 1 and Fig. 1 (after 50 cycles) for the A/CVP/1800-2700, B/ClQ5/1800-2600 and B/ClQ1/2000-2600 materials. Reasonably good linear correlations with R^2 values in the range 0.910–0.980 and 0.851–0.984 were attained for the interlayer spacing, d_{002}, and the crystal thickness, L_c, of these materials. In the case of the Raman parameter, I_D/I_t, the correlation was restricted to the A/CVP/1800-2700 and B/ClQ1/2000-2600 materials with R^2 of 0.899 and 0.957. Unlike the reversible capacity, no specific influence of the electrode material structure on the battery cyclability was observed. Thus, after the SEI formation, the intercalation of the lithium ions into the aromatic layers of all of the materials prepared was almost totally reversible (Table 1, Fig. 1). Their graphite-like structure as well as negligible porosity (Table 2), which was reported to influence the lithium insertion [24], can explained this behaviour. In a recent study, graphitized carbons of variable degree of crystallinity and morphology have also shown comparable retention capacity along galvanostatic cycling [12].

The dependence of the electrochemical intercalation of lithium in well-ordered (graphite-like) carbon materials prepared from different precursors on their XRD crystal structure has been previously studied by other authors [12–15]. The crystal thickness, L_c, was reported to be the most important factor affecting the extent of the reversible capacity. As in the work discussed here, a tendency of these materials capacity to increase with L_c was observed [13,15], but no specific correlation between the electrode capacity and the crystal thickness or other crystalline parameters of the materials was established in these studies. However, when graphite-like materials of high degree of crystallinity obtained from different precursors were considered, this tendency was not followed at all and thus, larger capacities were delivered by materials with lower [12] or similar [14] L_c values. In this sense, as mentioned above, A/CVP/2700 and B/ClQ5/2600 materials have provided reversible capacities similar to SG graphite with a much higher L_c crystal size (Table 1). Since the L_a crystal size calculated for SG graphite is also higher and as expected it shows a lower I_D/I_t, the good performance as electrodes in lithium-ion batteries of these high ordered carbon materials should be also related to other non structural factors. Among them, the influence of the graphite morphology on its electrochemical performance has been widely studied [12,13,25–29]. In an attempt to go insight this issue, the morphology of A/CVP/2700, B/ClQ5/2600 and SG was studied by SEM and the corresponding micrographs are given in Fig. 3. Unlike SG graphite of reference, both A/CVP/2700 and B/ClQ5/2600 materials have an irregular particle shape with no flakes. This type of particle morphology has been suggested to improve the battery performance through the formation of enough voids between the particles in the pressed electrode, thus allowing a good percolation of the electrolyte solution to reach all of the electrode active mass and therefore, the surface through which the Li intercalation occurs [26].

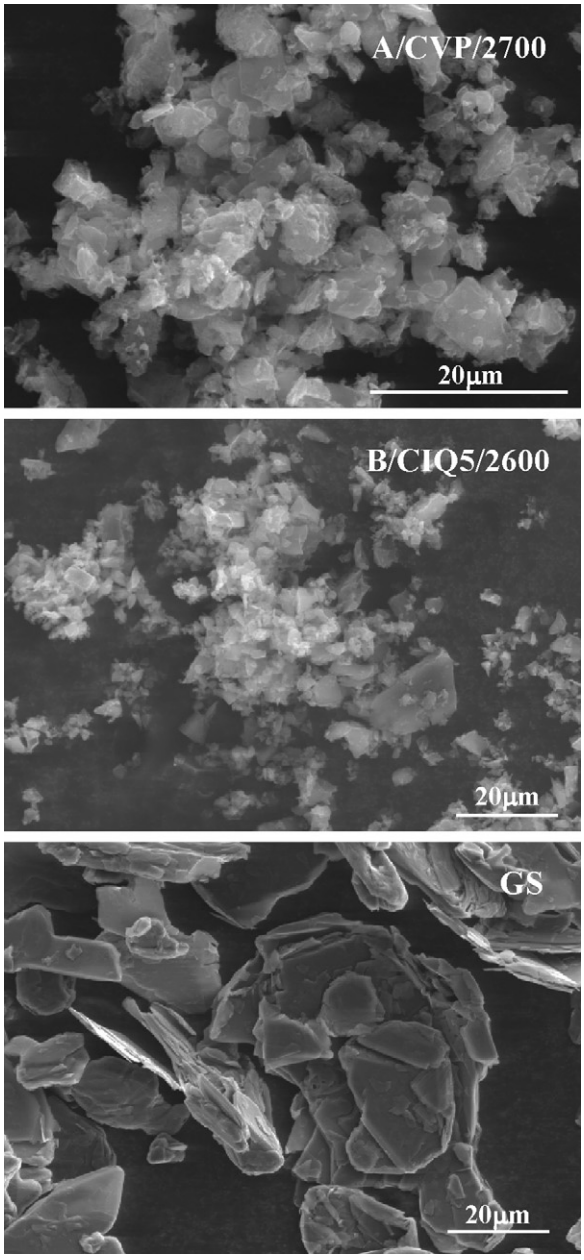

Fig. 3. SEM images of A/CVP/2700, B/ClQ5/2600 and SG materials.

The irreversible charge losses (irreversible capacity, C_{irr}) during the first discharge–charge cycle of the materials prepared are reported in Table 2. The absolute values of this electrochemical parameter are <150 mA hg^{-1}. Specifically, values of C_{irr} of 86 mA hg^{-1} (22%) and 142 mA hg^{-1} (32%) were, respectively, calculated for A/CVP/2700 and B/CIQ5/2600 which, as mentioned, have shown the best cycling behaviour with reversible capacities similar to SG graphite (Fig. 1). Unlike previous reported data [30–32], no relation between the BET specific surface area or the active surface area (ASA) as indirectly estimated from the structural parameters (ASA corresponds to the cumulated area of the different type of defects present on the carbon surface) and the irreversible consumption of Li could be established for the materials studied in this work, particularly when all of them are considered together (Tables 1 and 2).

4. Conclusions

The graphite-like materials prepared from the unburned carbon concentrates by high temperature treatment provided reversible capacities up to ~310 mA hg^{-1} after 50 discharge–charge cycles, these values being similar to those of oil-derived graphite used as reference. Moreover, they showed a remarkable stable capacity along cycling and low irreversible capacity. Apparently, both the high degree of crystallinity and the irregular particle shape with no flakes appear to contribute to the good anodic performance in lithium-ion batteries of these materials, thus making feasible their utilization to this end.

Acknowledgements

Financial support from the Spanish Ministry of Science and Innovation MICINN (Under Projects MAT2004-01094), and FICYT (Under Project PC07-014) is gratefully acknowledged. I. Cameán thanks MICINN for a personal grant to develop the work.

Appendix A. Supplementary data

Supplementary data associated with this article can be found, in the online version, at doi:10.1016/j.jpowsour.2011.01.041.

References

[1] M. Wakihara, Materials Science and Engineering R33 (2001) 109–134.
[2] D.W. Olson, Graphite, 2006 Mineral Year Book, U.S. Geological Survey, U. S. Department of Interior, Washington, 2007.
[3] M. Inagaki, in: P. Delhaès (Ed.), Graphite and Precursors, Gordon and Breach, Amsterdam, 2001, pp. 179–198.
[4] A. Oberlin, G. Terriere, Carbon 13 (1975) 367.
[5] R.M. Bustin, J.N. Rouzaud, J.V. Ross, Carbon 33 (1995) 679–691.
[6] J.V. Atria, F. Rusinko, H.H. Schobert, Energy & Fuels 16 (2002) 1343–1347.
[7] D. Gonzalez, M.A. Montes-Morán, I. Suarez-Ruiz, A.B. Garcia, Energy & Fuels 18 (2004) 365–370.
[8] D. Gonzalez, M.A. Montes-Morán, A.B. Garcia, Energy & Fuels 19 (2005) 263–269.
[9] I. Cameán, P. Lavela, J.L. Tirado, A.B. Garcia, Fuel 89 (2010) 986–991.
[10] M. Cabielles, M.A. Montes-Morán, A.B. Garcia, Energy & Fuels 22 (2008) 1239–1243.
[11] M. Cabielles, J.-N. Rouzaud, A.B. Garcia, Energy & Fuels 23 (2009) 942–950.
[12] J.C. Arrebola, A. Caballero, L. Hernán, J. Morales, Journal of the Electrochemical Society 156 (2009) A986–A992.
[13] M. Endo, C. Kim, K. Nishimura, T. Fujino, K. Miyashita, Carbon 38 (2000) 183–197.
[14] J.R. Dahn, A.K. Sleigh, H. Shi, J.N. Reimers, Q. Zhong, B.M. Way, Electrochimica Acta 38 (1993) 1179–1191.
[15] M. Endo, Y. Nishimura, T. Takahashi, K. Takeuchi, M.S. Dresselhaus, Journal of Physical Chemistry Solids 57 (1996) 725–728.
[16] Coal Facts. American Coal Ash Association (ACAA), 2010. www.acaa-usa.org.
[17] A. Cuesta, P. Dhamelincourt, J. Laureyns, A. Martinez-Alonso, J.M.D. Tascon, Journal of Materials Chemistry 8 (1998) 2875–2879.
[18] A. Cuesta, P. Dhamelincourt, J. Laureyns, A. Martinez-Alonso, J.M.D. Tascón, Carbon 32 (1994) 1523–1532.
[19] M.A. Montes-Morán, R.J. Young, Carbon 40 (2002) 845–855.
[20] A.F. Valdés, A.B. Garcia, Fuel 85 (2006) 607–614.
[21] J. Biscoe, B. Warren, Journal of Applied Physics 13 (1942) 364–371.
[22] T. Zheng, J.R. Dahn, Synthetic Metals 73 (1995) 1–7.
[23] F. Tuinstra, J.L. Koening, Journal of Chemical Physics 53 (1970) 1120–1126.
[24] F. Joho, B. Rykart, A. Blome, P. Novák, H. Wilhelm, M.E. Spahr, Journal of Power Sources 97–98 (2001) 78–82.
[25] P.G. Bruce, B. Scrosati, J.-M. Tarascon, Agewandte Chemie 47 (2008) 2930–2946.
[26] D. Aurbach, H. Teller, E. Levi, Journal of the Electrochemical Society 149 (2002) A1255–A1266.
[27] X. Wang, G.-S. Gai, Y.-F. Yang, W.-C. Shen, Powder Technology 181 (2008) 51–56.
[28] X.-L. Wu, Q. Liu, Y.-G. Guo, W.-G. Song, Electrochemistry Communications 11 (2008) 1468–1471.
[29] K. Zaghib, X. Song, A. Guerfi, R. Kostecki, K. Kinoshita, Journal of Power Sources 124 (2003) 505–512.
[30] D. Aurbach, H. Teller, M. Koltypin, E. Levi, Journal of Power Sources 119–121 (2003) 2–7.
[31] M. Winter, P. Novak, J. Monnier, Journal of the Electrochemical Society 145 (1998) 428–436.
[32] S.H. Ng, C. Vix-Gurtel, Ph. Bernardo, N. Tran, J. Ufheil, H. Buqa, J. Dentzer, R. Gadiou, M.E. Spahr, D. Goers, P. Novák, Carbon 47 (2009) 705–712.